

# Impact of meningeal uptake and partial volume correction techniques on [<sup>18</sup>F]MK-6240 binding in aMCI patients and healthy controls

Nathalie Mertens<sup>1</sup> , Laura Michiels<sup>2,3,4</sup> ,  
 Greet Vanderlinden<sup>1</sup>, Mathieu Vandenbulcke<sup>2,5</sup>,  
 Robin Lemmens<sup>2,3,4</sup>, Koen Van Laere<sup>1,6,\*</sup> and Michel Koole<sup>1,\*</sup>

## Abstract

[<sup>18</sup>F]MK-6240 is a second-generation tau PET-tracer to quantify neurofibrillary tangles in-vivo. However, individually variable levels of meningeal uptake induce spill-in-effects into the cortex, complicating [<sup>18</sup>F]MK-6240 PET quantification. Group SUVR differences between age-matched HC subgroups with varying extracerebral uptake (EC-low/mixed/high), and between aMCI and each HC subgroup were assessed without and with partial volume correction (PVC). Both Müller-Gartner (MG-)PVC and region-based voxelwise (RBV-)PVC, with the latter also correcting for extracerebral spill-in-effects, were implemented. Between HC groups, where no differences are to be expected, HC EC-high showed spill-in differences compared to HC EC-low when no PVC was applied while for MG-PVC, differences were reduced and, for RBV-PVC, no statistically significant differences were observed. Between aMCI and HC, cortical SUVR differences were statistically significant, both without and with PVC, but modulated by the varying meningeal uptake in HC subgroups when no PVC was applied. After applying PVC, correlations to clinical parameters improved and effect sizes between HC and aMCI increased, independent of the HC-subgroup. Therefore, appropriate PVC with correction for extracerebral spill-in-effects is recommended to minimize the impact of varying meningeal uptake on cortical differences between HC and aMCI.

## Keywords

[<sup>18</sup>F]MK-6240 PET quantification, amnesic mild cognitive impairment, healthy controls, meningeal uptake, partial volume correction

Received 24 August 2021; Revised 2 December 2021; Accepted 26 December 2021

## Introduction

The accumulation and regional spread of brain neurofibrillary tangles (NFTs) in Alzheimer's disease (AD) progresses through well-characterized pathological disease stages which are correlated to disease progression and clinical outcome as evaluated by neuropsychological tests (e.g., mini-mental state examination (MMSE) and Rey's auditory verbal learning test (RAVLT)).<sup>1</sup> *In vivo* tau positron emission tomography (PET) imaging of a variety of promising tau biomarkers has shown promise for early and differential diagnosis, as well as (therapy) monitoring of neurodegenerative disease progression.<sup>1–3</sup> First-generation tau tracers showed a

<sup>1</sup>Nuclear Medicine and Molecular Imaging, University Hospital and KU Leuven, Leuven, Belgium

<sup>2</sup>Department of Neurosciences, Experimental Neurology, KU Leuven – University of Leuven, Leuven, Belgium

<sup>3</sup>VIB, Center for Brain & Disease Research, Laboratory of Neurobiology, Leuven, Belgium

<sup>4</sup>Department of Neurology, University Hospitals Leuven, Leuven, Belgium

<sup>5</sup>Old-Age Psychiatry, University Hospital and KU Leuven, Leuven, Belgium

<sup>6</sup>Division of Nuclear Medicine, University Hospitals Leuven, Belgium

\*These authors contributed equally to this work.

## Corresponding author:

Nathalie Mertens, Department of Nuclear Medicine, University Hospitals Leuven, Herestraat 49, 3000 Leuven, Belgium.  
 Email: [nathalie.mertens@kuleuven.be](mailto:nathalie.mertens@kuleuven.be)

varying amount of off-target binding *in vivo* and relatively low signal to noise ratio.<sup>4–6</sup> Meanwhile, second-generation tau PET tracers such as [<sup>18</sup>F]MK-6240 show improved tracer characteristics with higher specific binding to NFTs and no appreciable intracerebral off-target binding.<sup>7</sup> Several landmark studies have used [<sup>18</sup>F]MK-6240 to quantify NFTs in patients with amnesic mild cognitive impairment (aMCI) and AD<sup>8–13</sup> and have shown its correspondence to pathological stages.<sup>14</sup> Although [<sup>18</sup>F]MK-6240 displays very low off-target signal in brain parenchyma,<sup>15</sup> varying levels of meningeal tracer uptake have been noticed, confirmed by postmortem autoradiography studies.<sup>16–18</sup> Even though the exact nature of the uptake is still under debate, this varying extracerebral (EC) tracer uptake causes partial volume effects (PVE) due to spill-over of this activity to nearby cortical regions which may hamper accurate quantification and hinder optimal interpretation of [<sup>18</sup>F]MK-6240 PET scans.

The aim of this study was to investigate the impact of meningeal uptake spill-in on the quantification of [<sup>18</sup>F]MK-6240 PET and to evaluate partial volume correction (PVC) techniques to correct for this. We hypothesized that the inclusion of an extracerebral compartment would improve modelling of varying meningeal uptake and therefore reduce the corresponding spill-in effects. We compared a PVC method which does not take extracerebral uptake into account (voxelwise Müller-Gartner (MG) correcting for PVE between white (WM) and gray matter (GM), assuming homogeneous WM uptake), with a region-based voxelwise (RBV) PVC method which also includes extracerebral compartments (including extracerebral cerebrospinal fluid (CSF), skull and skin tissue).

As a first objective, we compared the effect of meningeal spill-in in HC groups with low and high meningeal uptake without and with PVC, assuming that on an age-matched group-level, no differences in [<sup>18</sup>F]MK-6240 uptake are to be expected. As second objective, meningeal spill-in effects and the effect of different PVC approaches on observed group differences between aMCI and HC was evaluated to relate the effect to the observed known differences for aMCI patients. Thirdly, the effect of PVC on correlations to clinical symptomatology was evaluated.

## Material and methods

### [<sup>18</sup>F]MK-6240 PET-MR imaging

For this study, all subjects underwent a simultaneous [<sup>18</sup>F]MK-6240 PET-magnetic resonance (MR) scan (Signa PET-MR, General Electric Healthcare), acquired 90–120 minutes post tracer injection. Synthesis of tracer was performed as previously

described.<sup>19</sup> For the PET scan, HC and aMCI subjects received a tracer dose of  $138 \pm 26$  MBq and  $155 \pm 13$  MBq respectively.

All PET data were acquired in list mode and rebinned into 6 frames of 5 minutes. Sinograms were corrected for deadtime, randoms and scatter while a zero-echo time (ZTE) MR-based attenuation map was used for the attenuation correction.<sup>20</sup> Each frame was reconstructed using ordered subsets expectation maximization (OSEM, 28 subsets, 4 iterations) and included time-of-flight (TOF) information, resolution modeling and a Gaussian post-smoothing with a full width half maximum (FWHM) of 4 mm.

The multiframe PET data were rescaled to standardized uptake values (SUV) and corrected for motion by aligning each frame to the first frame using a rigid transformation. Next, frames were averaged to obtain a static SUV PET image. For PVE corrected data, the specific PVC approach was applied to the static SUV values such that uptake in the reference region was also corrected for PVE. Finally, SUV PET data were converted to standardized uptake value ratio (SUVR) images relative to whole cerebellar GM.<sup>10,15</sup>

Simultaneous with the PET acquisition, a 3D volumetric 3 Tesla T1 weighted BRAVO MR sequence was acquired (Plane: sagittal; TE: 3.2 ms; TR: 8.5 ms; TI: 450 ms; flip angle: 12°; receiver bandwidth: 31.2 kHz; NEX: 1; voxelsize:  $1 \times 1 \times 1$  mm) followed by a 3D T2 weighted FLAIR sequence (Plane: sagittal; TE: 137 ms; TR: 8500 ms; TI: 2298 ms; receiver bandwidth: 31.25 kHz; NEX: 1; voxelsize:  $0.7 \times 1 \times 1$  mm).

In addition, amyloid status of all subjects  $\geq 50$  years old was confirmed using [<sup>11</sup>C]Pittsburgh compound B (PiB) PET, with the [<sup>11</sup>C]PiB PET scan dichotomously interpreted as positive or negative based on the visual reading by a nuclear medicine specialist.<sup>1</sup>

### Subject groups

For the aMCI group, 10 aMCI patients (6 M/4 F; age  $70 \pm 5$  years, range 63–79 years; MMSE score range 22–28, 9 out of 10 amyloid-positive) were included. To define the different HC groups, a k-means clustering algorithm was used to classify 40 HC into two groups with low and high extracerebral tracer uptake respectively (kmeans1d toolbox, Python library).<sup>21,22</sup> Classification was done based on the mean standardized uptake value ratio (SUVR) of the skull parcel (Freesurfer v6.0, Laboratory for Computational Neuroimaging v6.0, Boston, USA) relative to the whole cerebellar GM as this parcel included the meninges and was therefore considered indicative for the level of meningeal uptake. From these two clusters, three groups of each 10 HC were defined: 10 HC with low meningeal uptake (HC EC-low), 10 HC with high

meningeal uptake (HC EC-high), and a mixed group containing 5 HC from the HC EC-low and HC EC-high group (HC EC-mixed). To eliminate potential age effects on [<sup>18</sup>F]MK-6240 uptake,<sup>23</sup> subjects within each HC group were selected to ensure age-match between the different HC subgroups, as well as between each HC subgroups and the aMCI group (see Supplementary Figure 1). This resulted in the inclusion of 20 age-matched HC (9 M/11 F; age  $68 \pm 9$  years, range 49–83 years; MMSE score range 28–30, 4 out of 20 amyloid-positive) with either low or high extracerebral tracer uptake.

Detailed demographics for the aMCI patients can be found in<sup>1</sup> and for the HC.<sup>24</sup> The study was conducted at the University Hospital Leuven, Belgium, approved by the local Ethics Committee (University Hospitals Leuven/KU Leuven) and each subject signed a written informed consent before enrollment. All procedures performed in studies involving human participants were in accordance with the ethical standards of the institutional and/or national research committee and with the 1964 Helsinki declaration and its later amendments or comparable ethical standards. All subjects signed informed consent before entering the study.

### PVC methods

Two PVC methods were implemented in Python3.8. For both PVC methods, a 3D isotropic Gaussian kernel with a FWHM of 6.5 mm was used to model the PET resolution.

First, a voxelwise Müller-Gartner (MG) PVC method<sup>25</sup> was implemented to estimate true GM uptake by taking into account GM and WM uptake while assuming homogeneous tracer uptake in WM. Subject specific tissue probability maps for GM, WM and CSF were derived from the T1 weighted MR images using the CAT12 toolbox (SPM12; Wellcome Department of Cognitive Neurology, London, UK).<sup>26,27</sup>

Second, a region-based voxelwise (RBV) PVC method<sup>28</sup> was implemented to estimate PVE corrected PET images by taking into account anatomical parcellation which also includes extracerebral regions such as extracerebral CSF, skull and head tissue. Parcellation was obtained with FreeSurfer using both the T1 and T2 weighted FLAIR MR images. The cortical parcellation was based on the Desikan-Killiany atlas<sup>29,30</sup> while subcortical structures were parcellated as described by Fischl et al.<sup>31</sup> For a more robust RBV estimation, certain parcels were merged into larger regions ( $n = 42$ ; see Supplementary Table 1).

### Statistical analysis

For the VOI-based analysis, 9 composite brain regions were created from the FreeSurfer parcellation including the temporal, frontal, occipital, parietal, cingulate and mesotemporal cortex as well as the caudate nucleus, putamen and thalamus. Even though no tau load is expected in subcortical regions, SUVR differences were also assessed in these regions to validate the PVC methods. Additionally, a composite GM VOI containing all GM regions was created. For each VOI, normality of the SUVR distributions was verified with a Shapiro-Wilk test ( $\alpha = 0.05$ ). Group SUVR differences between HC EC-low and HC EC-high, as well as between aMCI and the HC groups, were assessed by a Welch's t-test or a Mann-Whitney U test while using a Bonferroni-corrected significance level of  $\alpha = 0.05$ . Effect sizes were calculated for each region as mean aMCI to HC SUVR ratios (aMCI SUVR/HC SUVR) and were compared using a paired t-test. A Spearman correlation ( $r_s$ ) was used to evaluate the relationship between MMSE and SUVR in the mesotemporal region for the aMCI group. All statistics were performed using the statistics module of the SciPy software (Scientific computing tools for Python) in Python3.8, both without and with PVC.

A complementary voxel-based analysis was performed using the SUVR maps (SPM12;  $p_{\text{height, uncorr}} < 0.001$  and  $p_{\text{cluster, FWE-corr}} < 0.05$ ) both without and with PVC. SUVR images were first masked with individual GM masks (threshold 0.95) to prevent smoothing of meningeal uptake into the cortex and then spatially normalized using CAT12. Images were smoothed prior to the statistical analysis using an isotropic Gaussian kernel with 8 mm FWHM. In addition, an explicit binary mask, created by averaging the normalized and binarized GM and CSF probability maps of all HC (threshold 0.40), was used for the statistical analysis.

## Results

### HC subgroups

Clustering of HC cohort ( $n = 40$ ) into two groups based on extracerebral SUVR, resulted in a group with lower extracerebral SUVR of  $1.08 \pm 0.14$  ( $n = 22$ ) and a group with a higher extracerebral SUVR uptake of  $1.54 \pm 0.21$  ( $n = 18$ ) respectively. The corresponding threshold for separating the two groups was 1.31. Representative SUVR images of two HC and two aMCI patients with low and high meningeal uptake are presented in Figure 1.

Age-matched HC EC-low and HC EC-high groups of 10 HC each resulted in a corresponding

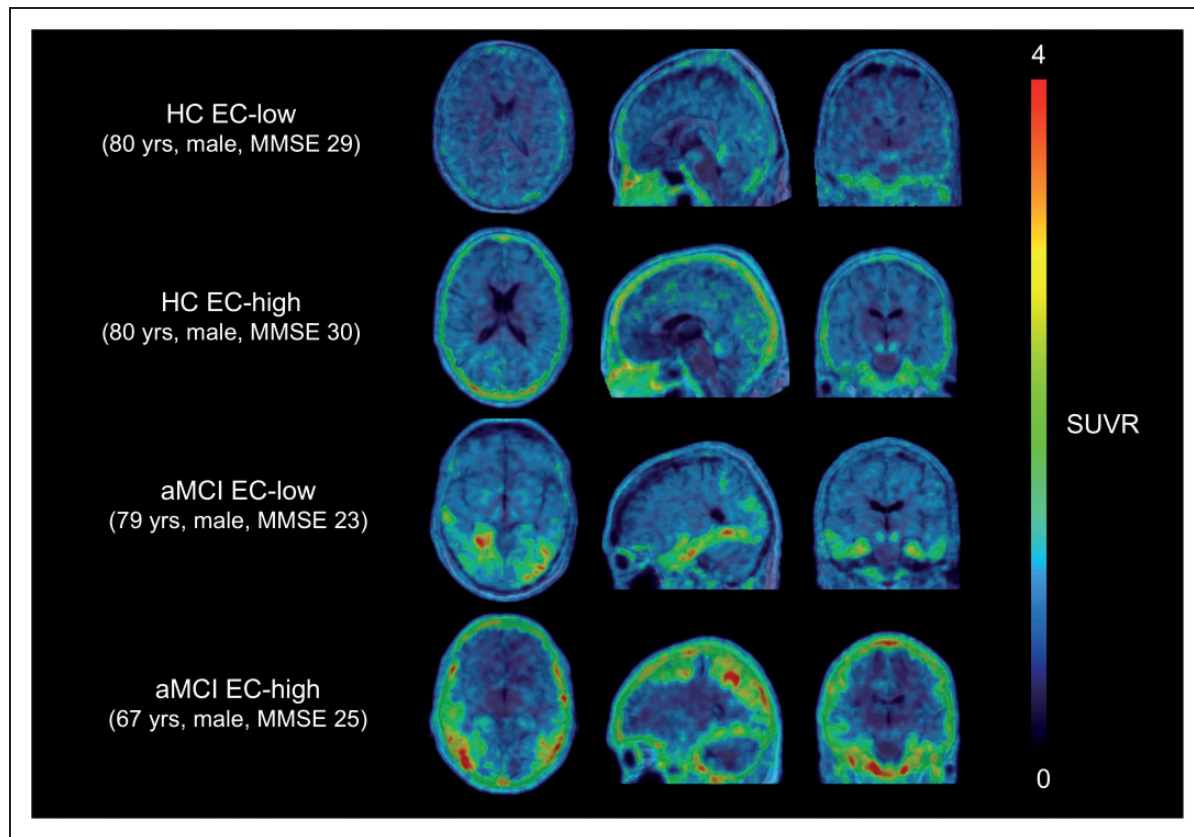


**Figure 1.** [ $^{18}\text{F}$ ]MK-6240 SUVR image overlaid on the corresponding 3D T1 weighted MR image in MNI space of two HC and aMCI subjects with low and high meningeal tracer uptake respectively. SUVR: standardized uptake value ratio; MR: magnetic resonance; MNI: Montreal Neurological Institute; HC: healthy controls; aMCI: amnesic mild cognitive impairment; EC: extracerebral; MMSE: mini-mental state examination.

**Table 1.** Demographics and [ $^{18}\text{F}$ ]MK-6240 uptake values of different groups.

	Age (years)	Gender	Amyloid-positive (%)	Range MMSE score	EC SUVR
HC (n = 40)	57 ± 19	19M/21F	4 (10%)	28–30	1.29 ± 0.29
HC EC-low (n = 22)	60 ± 19	13M/9F	2 (9%)	28–30	1.08 ± 0.14
HC EC-high (n = 18)	54 ± 18	6M/12F	2 (11%)	28–30	1.54 ± 0.21
Age matched (n = 10)					
aMCI	70 ± 5	6M/4F	9 (90%)	22–28	1.12 ± 0.31
HC EC-low	69 ± 9	6M/4F	2 (20%)	28–30	1.01 ± 0.11
HC EC-high	68 ± 9	3M/7F	2 (20%)	28–30	1.43 ± 0.10
HC EC-mixed	67 ± 6	5M/5F	1 (10%)	28–30	1.23 ± 0.28

Values are represented as mean ± standard deviation. M: male; F: female; SUVR: standardized uptake value ratio; HC: healthy controls; EC: extracerebral; aMCI: amnesic mild cognitive impairment; MMSE: Mini-Mental State Examination.

extracerebral SUVR of  $1.01 \pm 0.11$  and  $1.43 \pm 0.10$  respectively. In addition, 5 HC were selected from each group to form an age-matched HC EC-mixed group, resulting in a group with extracerebral SUVR of  $1.23 \pm 0.28$ . For HC EC-low and HC EC-high, 2 out of 10 subjects were amyloid-positive, while only one subject was amyloid-positive in the HC EC-mixed group. An overview of all HC subgroups is given in Table 1.

### Group differences between HC subgroups

Mean regional no-PVC and PVC SUVR values of HC EC-low and HC EC-high are shown in Figure 2 and Table 2, together with p-values for group comparisons.

For the cortical no-PVC SUVR data, HC EC-high showed significant higher SUVR compared to HC EC-low with significant differences found in the temporal,

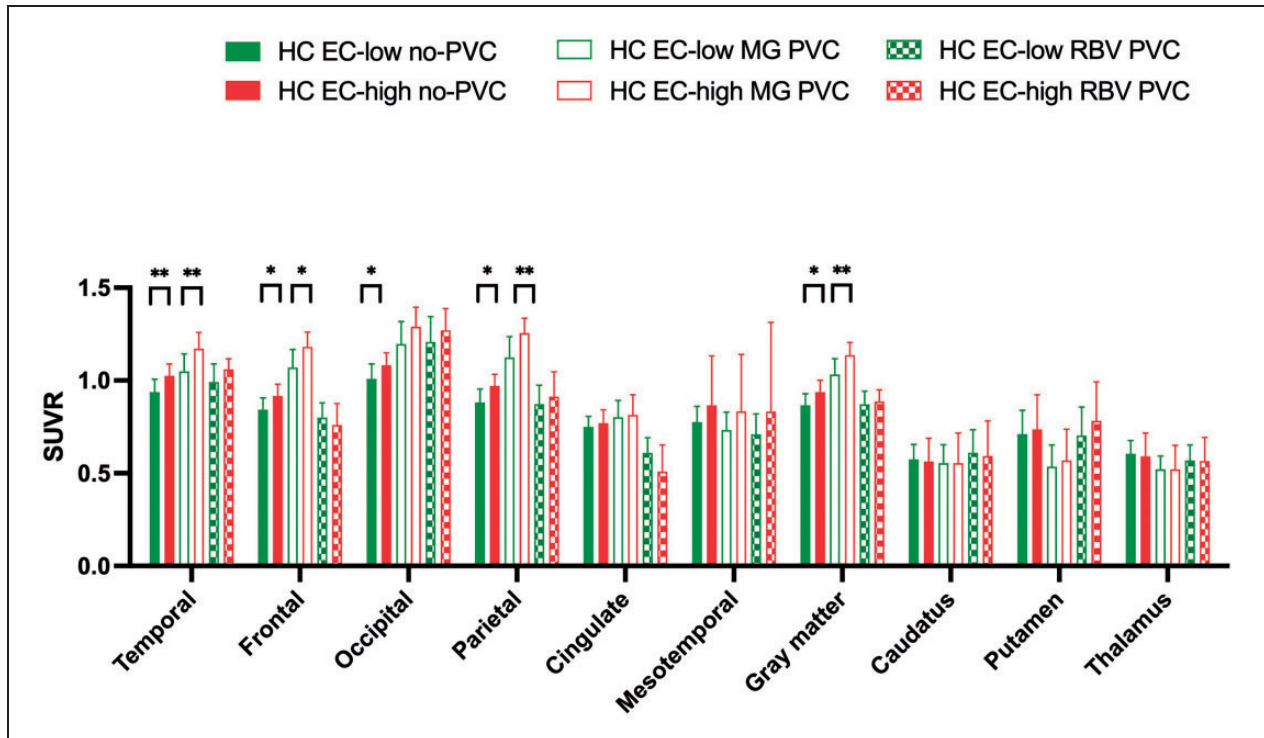


**Figure 2.** Mean regional [ $^{18}\text{F}$ ]MK-6240 SUVR values of 10 HC with low (green) and high (red) extracerebral tracer uptake respectively. Filled bars indicate SUVR values without PVC; empty bars indicate SUVR values with MG PVC; pattern bars indicate SUVR values with RBV PVC taking into account extracerebral tracer uptake. Significant differences are presented by \*( $p < 0.05$ ); \*\*( $p < 0.01$ ). SUVR: standardized uptake value ratio; HC: healthy controls; EC: extracerebral; MG: Müller-Gartner; PVC: partial volume correction; RBV: region-based voxelwise.

frontal, occipital, parietal cortex and the composite GM region.

After PVC, cortical MG PVC SUVR values were significantly higher for HC EC-high compared to HC EC-low in the temporal, frontal and parietal cortex, as well as in the composite GM region, but not in the occipital cortex. On the other hand, no significant cortical differences were found for RBV PVC SUVR between HC EC-low and HC EC-high.

For the subcortical regions, no significant differences were detected between HC EC-low and HC EC-high for both no-PVC and PVC SUVR values.

All VOI-based results were confirmed by a voxel-based comparison between HC EC-low and HC EC-high using no-PVC and PVC SUVR maps (see Supplementary Figure 2).

### Group differences between aMCI and HC subgroups

Nine out of 10 aMCI patients showed low meningeal uptake as determined by the dichotomization threshold (Table 1). Representative SUVR images of a 79-years and 67-years old male aMCI with low and high meningeal uptake respectively are presented in Figure 1.

Table 2 presents the mean regional SUVR values without and with PVC for the aMCI group and HC, where the three HC groups with low, mixed and high meningeal uptake, respectively, were taken as comparator.

For the uncorrected SUVR data, comparison between aMCI and the different HC groups showed inconsistent significant regional differences (Table 2). When comparing aMCI with HC EC-high, less regional significant differences were observed compared to group differences between aMCI and HC EC-mixed or HC EC-low.

After applying PVC, significant group differences between the aMCI group and the different HC groups were found in all cortical regions, with similar findings for both the MG and RBV PVC method (Table 2). Overall, regional SUVR in aMCI showed an increased variance for both PVC methods compared to the HC subgroups (average regional coefficient of variation aMCI vs HC EC-low: 34% vs 10% ( $p = 0.002$ ), 31% vs 13% ( $p = 0.006$ ) and 52% vs 14% ( $p = 0.002$ ) for no-PVC, MG PVC and RBV PVC respectively).

For the subcortical regions, no significant differences were detected between aMCI and the different HC groups, both for no-PVC and PVC SUVR data.

**Table 2.** Regional [ $^{18}\text{F}$ ]MK-6240 SUVR values (mean  $\pm$  standard deviation) of 10 aMCI patients and three groups of 10 HC with low, mixed and high extracerebral tracer uptake respectively. SUVR values are presented without PVC (no-PVC); with MG PVC, and with RBV PVC taking into account extracerebral tracer uptake.

	SUVR				p-value			
	aMCI	HC EC-low	HC EC-mixed	HC EC-high	HC EC-low versus HC EC-high	aMCI versus HC EC-low	aMCI versus HC EC-mixed	aMCI versus HC EC-high
<b>no-PVC</b>								
Temporal cortex	1.42 $\pm$ 0.72	0.94 $\pm$ 0.07	0.98 $\pm$ 0.07	1.03 $\pm$ 0.06	<b>0.0021</b>	<b>0.0015</b>	<b>0.0089</b>	0.063
Frontal cortex	1.16 $\pm$ 0.47	0.84 $\pm$ 0.06	0.89 $\pm$ 0.07	0.92 $\pm$ 0.06	<b>0.019</b>	<b>0.0052</b>	<b>0.015</b>	<b>0.023</b>
Occipital cortex	1.28 $\pm$ 0.38	1.01 $\pm$ 0.08	1.02 $\pm$ 0.07	1.08 $\pm$ 0.07	<b>0.016</b>	0.075	0.063	0.74
Parietal cortex	1.26 $\pm$ 0.63	0.88 $\pm$ 0.07	0.92 $\pm$ 0.06	0.97 $\pm$ 0.06	<b>0.011</b>	0.043	0.25	0.97
Cingulate cortex	1.01 $\pm$ 0.46	0.75 $\pm$ 0.06	0.76 $\pm$ 0.07	0.77 $\pm$ 0.07	0.54	<b>0.0029</b>	<b>0.0068</b>	<b>0.023</b>
Mesotemporal cortex	1.34 $\pm$ 0.49	0.78 $\pm$ 0.08	0.79 $\pm$ 0.10	0.87 $\pm$ 0.27	0.48	<b>0.0052</b>	<b>0.0060</b>	<b>0.0089</b>
Caudate nucleus	0.55 $\pm$ 0.11	0.57 $\pm$ 0.08	0.57 $\pm$ 0.08	0.56 $\pm$ 0.13	0.68	0.65	0.69	0.85
Putamen	0.73 $\pm$ 0.10	0.71 $\pm$ 0.13	0.71 $\pm$ 0.14	0.74 $\pm$ 0.19	0.54	0.70	0.75	0.74
Thalamus	0.62 $\pm$ 0.08	0.60 $\pm$ 0.07	0.59 $\pm$ 0.08	0.59 $\pm$ 0.13	0.53	0.73	0.52	0.35
Gray matter	1.20 $\pm$ 0.48	0.87 $\pm$ 0.06	0.90 $\pm$ 0.06	0.94 $\pm$ 0.06	<b>0.019</b>	<b>0.0015</b>	<b>0.0039</b>	<b>0.035</b>
<b>MG PVC</b>								
Temporal cortex	1.91 $\pm$ 0.90	1.05 $\pm$ 0.09	1.10 $\pm$ 0.11	1.17 $\pm$ 0.09	<b>0.0018</b>	<b>7.6 <math>\times 10^{-5}</math></b>	<b>0.00073</b>	<b>0.0068</b>
Frontal cortex	1.56 $\pm$ 0.71	1.07 $\pm$ 0.10	1.14 $\pm$ 0.09	1.18 $\pm$ 0.08	<b>0.013</b>	<b>0.00073</b>	<b>0.0052</b>	<b>0.019</b>
Occipital cortex	1.88 $\pm$ 0.57	1.20 $\pm$ 0.12	1.20 $\pm$ 0.11	1.29 $\pm$ 0.10	0.097	<b>0.0044</b>	<b>0.0047</b>	<b>0.0099</b>
Parietal cortex	1.99 $\pm$ 0.82	1.12 $\pm$ 0.11	1.18 $\pm$ 0.09	1.26 $\pm$ 0.08	<b>0.0058</b>	<b>0.00032</b>	<b>0.0015</b>	<b>0.015</b>
Cingulate cortex	1.25 $\pm$ 0.12	0.80 $\pm$ 0.09	0.79 $\pm$ 0.11	0.82 $\pm$ 0.11	0.77	<b>4.3 <math>\times 10^{-5}</math></b>	<b>7.6 <math>\times 10^{-5}</math></b>	<b>7.6 <math>\times 10^{-5}</math></b>
Mesotemporal cortex	1.61 $\pm$ 0.63	0.73 $\pm$ 0.10	0.72 $\pm$ 0.10	0.83 $\pm$ 0.31	0.48	<b>0.0016</b>	<b>0.0015</b>	<b>0.0011</b>
Caudate nucleus	0.64 $\pm$ 0.12	0.56 $\pm$ 0.10	0.55 $\pm$ 0.10	0.56 $\pm$ 0.16	0.74	0.11	0.086	0.12
Putamen	0.64 $\pm$ 0.13	0.54 $\pm$ 0.12	0.54 $\pm$ 0.13	0.57 $\pm$ 0.17	0.44	0.069	0.084	0.41
Thalamus	0.56 $\pm$ 0.10	0.52 $\pm$ 0.07	0.51 $\pm$ 0.08	0.52 $\pm$ 0.13	0.97	0.36	0.23	0.58
Gray matter	1.67 $\pm$ 0.66	1.03 $\pm$ 0.09	1.08 $\pm$ 0.08	1.14 $\pm$ 0.07	<b>0.0045</b>	<b>0.00013</b>	<b>0.00049</b>	<b>0.0068</b>
<b>RBV PVC</b>								
Temporal cortex	2.18 $\pm$ 1.51	0.99 $\pm$ 0.10	1.04 $\pm$ 0.08	1.06 $\pm$ 0.06	0.080	<b>0.0011</b>	<b>0.0015</b>	<b>0.0021</b>
Frontal cortex	1.32 $\pm$ 1.06	0.80 $\pm$ 0.08	0.82 $\pm$ 0.09	0.76 $\pm$ 0.12	0.63	<b>0.0089</b>	<b>0.015</b>	<b>0.0039</b>
Occipital cortex	2.00 $\pm$ 0.76	1.21 $\pm$ 0.14	1.18 $\pm$ 0.09	1.27 $\pm$ 0.12	0.29	<b>0.0079</b>	<b>0.0068</b>	<b>0.012</b>
Parietal cortex	1.96 $\pm$ 1.27	0.87 $\pm$ 0.10	0.89 $\pm$ 0.10	0.91 $\pm$ 0.13	0.46	<b>0.00032</b>	<b>0.00049</b>	<b>0.0029</b>
Cingulate cortex	1.15 $\pm$ 0.96	0.61 $\pm$ 0.08	0.54 $\pm$ 0.15	0.51 $\pm$ 0.14	0.12	<b>0.019</b>	<b>0.0068</b>	<b>0.0029</b>
Mesotemporal cortex	2.14 $\pm$ 1.14	0.71 $\pm$ 0.11	0.71 $\pm$ 0.14	0.83 $\pm$ 0.48	0.80	<b>0.0031</b>	<b>0.0031</b>	<b>0.0029</b>
Caudate nucleus	0.67 $\pm$ 0.19	0.61 $\pm$ 0.12	0.61 $\pm$ 0.13	0.59 $\pm$ 0.19	0.63	0.32	0.32	0.22
Putamen	0.90 $\pm$ 0.17	0.70 $\pm$ 0.16	0.73 $\pm$ 0.17	0.78 $\pm$ 0.21	0.35	0.79	0.97	0.57
Thalamus	0.62 $\pm$ 0.12	0.57 $\pm$ 0.08	0.55 $\pm$ 0.09	0.57 $\pm$ 0.13	0.53	0.26	0.14	0.25
Gray matter	1.66 $\pm$ 0.99	0.87 $\pm$ 0.07	0.88 $\pm$ 0.06	0.89 $\pm$ 0.06	0.62	<b>0.0011</b>	<b>0.0015</b>	<b>0.0021</b>

P-values from VOI-based group comparisons are also reported, with significant p-values in bold. SUVR: standardized uptake value ratio, aMCI: amnesic mild cognitive impairment; HC: healthy controls; EC: extracerebral; MG: Müller-Gartner; PVC: partial volume correction; RBV: region-based voxelwise.

These results were confirmed by a voxel-based comparison between aMCI and the HC subgroups, showing inconsistent group differences in uncorrected SUVR maps. In contrast, after applying PVC, more consistent group differences between aMCI and the different HC groups were detected (Figure 3).

### Regional effect sizes between aMCI and HC subgroups

Regional effect sizes between aMCI and different HC groups are given in Table 3. Overall, effect sizes between aMCI and HC groups increased after PVC

compared to no-PVC SUVR data ( $1.27 \pm 0.21$  vs  $1.49 \pm 0.31$ , a 17% increase,  $p = 3.9 \times 10^{-11}$  and  $1.27 \pm 0.21$  vs  $1.79 \pm 0.55$ , a 41% increase,  $p = 5.4 \times 10^{-9}$  for no-PVC compared with MG and RBV PVC respectively). Between PVC methods, RBV PVC also showed higher effect sizes compared to MG PVC ( $p = 7.3 \times 10^{-7}$ ).

### Correlation between medial temporal tau load and MMSE in aMCI

PVC SUVR data showed a highly significant and strong correlation, which was similar for both PVC

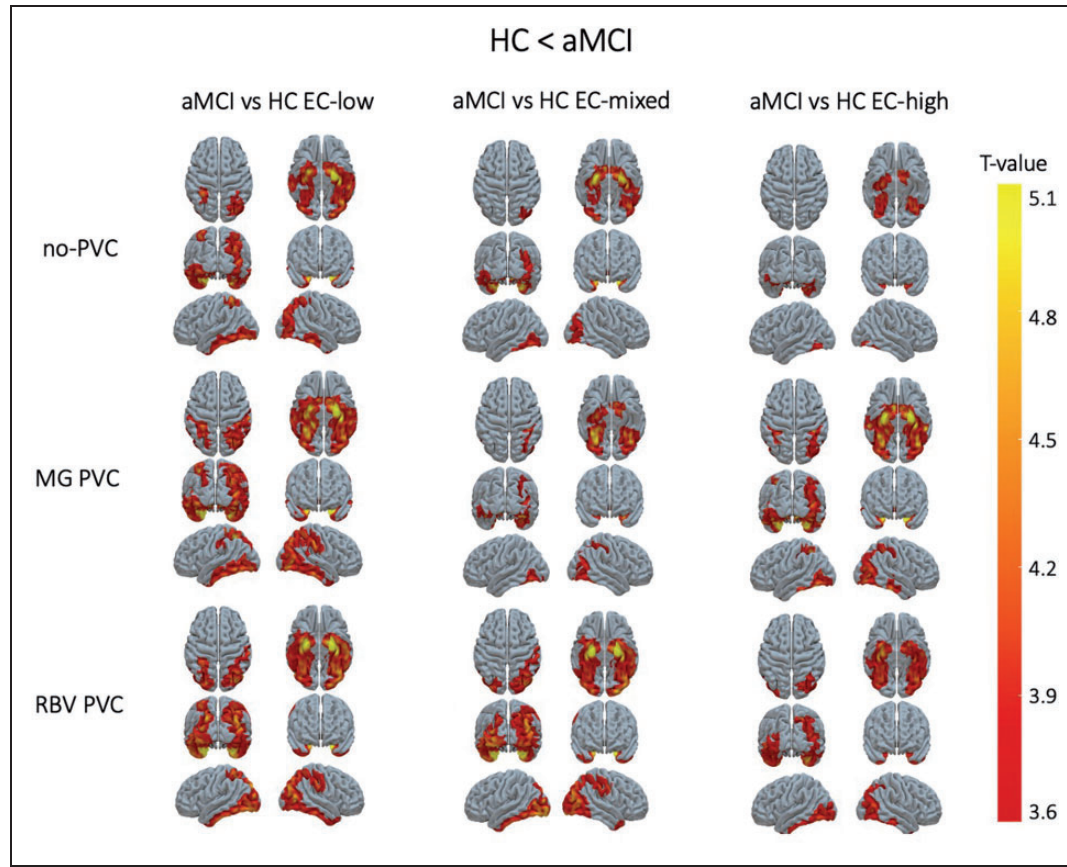


**Figure 3.** T-statistical maps of significant clusters rendered on the cortical surface for in the voxel-based comparison between [ $^{18}\text{F}$ ]MK-6240 SUVR maps of aMCI patients with HC with low, mixed and high extracerebral tracer uptake respectively using uncorrected SUVR maps (upper), PVC corrected SUVR maps using a MG PVC method which does not correct for PVE of extracerebral tracer uptake (middle) and PVC corrected SUVR maps using an RBV PVC method which also corrects for PVE of extracerebral tracer uptake (lower). SUVR: standardized uptake value ratio, aMCI: amnesic mild cognitive impairment, HC: healthy controls; EC: extracerebral; MG: Müller-Gartner; PVC: partial volume correction; RBV: region-based voxelwise.

**Table 3.** Regional effect sizes for 10 aMCI patients and 10 HC with respectively low (HC EC-low), mixed (HC EC-mixed) and high (HC EC-high) extracerebral [ $^{18}\text{F}$ ]MK-6240 uptake.

Effect size	aMCI vs HC EC-low			aMCI vs HC EC-mixed			aMCI vs HC EC-high		
	no-PVC	MG PVC	RBV PVC	no-PVC	MG PVC	RBV PVC	no-PVC	MG PVC	RBV PVC
Temporal cortex	1.52	1.82	2.20	1.45	1.73	2.10	1.39	1.63	2.06
Frontal cortex	1.38	1.46	1.65	1.30	1.37	1.62	1.27	1.32	1.74
Occipital cortex	1.27	1.57	1.66	1.26	1.56	1.69	1.18	1.46	1.58
Parietal cortex	1.43	1.77	2.24	1.37	1.69	2.21	1.30	1.58	2.14
Cingulate cortex	1.34	1.55	1.89	1.33	1.57	2.12	1.31	1.53	2.26
Mesotemporal cortex	1.73	2.20	3.02	1.70	2.22	3.01	1.55	1.93	2.57
Caudate nucleus	0.96	1.15	1.10	0.97	1.16	1.11	0.98	1.15	1.14
Putamen	1.03	1.20	1.28	1.02	1.19	1.23	0.99	1.13	1.15
Thalamus	1.02	1.07	1.10	1.04	1.10	1.13	1.04	1.07	1.10
Gray matter	1.39	1.62	1.90	1.34	1.55	1.87	1.28	1.47	1.87

Effect sizes were calculated by using SUVR data without PVC (no-PVC); with MG PVC, and with RBV PVC taking into account spill-in of extracerebral tracer uptake. aMCI: amnesic mild cognitive impairment, HC: healthy controls; EC: extracerebral; SUVR: standardized uptake value ratio; PVC: partial volume correction; MG: Müller-Gartner; RBV: region-based voxelwise.

methods ( $r_{p, MG\ PVC} = -0.82$ ,  $p = 0.004$  and  $r_{p, RBV\ PVC} = -0.81$ ,  $p = 0.005$ ). For no-PVC SUVR data, the correlation was slightly weaker, but it remained significant ( $r_{p, no-PVC} = -0.72$ ,  $p = 0.02$ ) (see Supplementary Figure 3).

## Discussion

In this study, we evaluated the impact of meningeal uptake on differences in cortical [ $^{18}F$ ]MK-6240 SUVR between HC and patients with aMCI. This off-target extracerebral tracer uptake has been reported by different groups, but thus far, no thorough evaluation of these spill-over effects, or of methods to reduce its impact have been described.

Our results clearly showed a significant impact of varying meningeal uptake on cortical [ $^{18}F$ ]MK-6240 SUVR data as significant differences were found in cortical brain areas between age-matched HC with low and high extracerebral tracer uptake. Also, group differences between aMCI patients and HC were dependent on the varying level of meningeal uptake in the HC group. As expected, consistently higher levels of extracerebral tracer uptake in the HC group resulted in a positive bias of the cortical [ $^{18}F$ ]MK-6240 SUVR of HC such that less cortical regions were found to be significantly different compared to an age-matched aMCI group, decreasing sensitivity to detect group differences. Additionally, we demonstrated that the impact of varying meningeal uptake in HC was only observed for cortical regions and not for the subcortical regions as these are not influenced by PVE of meningeal uptake. We also considered a mixed HC group as a HC group with only low or only high meningeal uptake is not to be expected when HC are randomly selected. Since almost 50% of all HC demonstrated high meningeal uptake, we defined a mixed group with 50% of the HC having high meningeal uptake and the other half demonstrating low meningeal uptake. This HC EC-mixed group was also used in the study by Vanhaute et al.<sup>1</sup> where aMCI was compared with HC in the context of a multi-tracer PET study. By including HC with varying meningeal uptake, we assumed that extracerebral SUVR would have less impact on cortical group differences between HC and aMCI because of increased variability. However, this increased variability in extracerebral uptake also induces an increased variability in cortical uptake, such that group differences between this mixed HC group and aMCI could still be improved by applying PVC.

After applying a PVC method which includes a correction for extracerebral spill-in effects, significant differences between two cohorts of age-matched HC with varying level of meningeal uptake were no longer

observed. In addition, group differences between aMCI and HC groups with different levels of meningeal uptake were found to be more robust, indicating independence of the composition of the HC group regarding levels of meningeal uptake.

These findings are in line with previous first-generation tau PET studies, which already showed the potential of PVC to minimize PVE caused by off-target tracer uptake. Indeed, PVE in subcortical regions of monoamine oxidases (MAO) off-target [ $^{18}F$ ]flortaucipir uptake were reduced after PVC.<sup>32,33</sup>

In terms of PVC, no significant differences were found between two cohorts of HC with low and high meningeal uptake using RBV PVC, while the MG PVC method did not eliminate group differences. This can be explained by the MG PVC method correcting only for activity concentrations in proportion to tissue type while RBV PVC applies a region-based voxelwise correction. Meanwhile, group differences between aMCI patients and HC with varying meningeal uptake, were less dependent on the PVC method as both the MG and RBV PVC showed similar VOI- and voxel-based differences. For the HC, cortical SUVR are mainly driven by meningeal spill-in as only non-specific [ $^{18}F$ ]MK-6240 uptake is expected in the cortex for these subjects. In contrast, for the aMCI group where specific, pathological cortical [ $^{18}F$ ]MK-6240 uptake is present, PVE was also driven by spill-in and spill-over effects between WM and GM tissue.

In our data set, low meningeal uptake was observed in the aMCI group as 9 out of 10 aMCI patients had skull SUVR below the HC-based dichotomization threshold, minimizing the impact of varying meningeal uptake in this group. This may be a statistical anomaly on the relatively small aMCI group, therefore the RBV PVC method which also corrects for extracerebral tracer uptake and thus takes into account PVE of meningeal uptake, is considered to be the preferred method for [ $^{18}F$ ]MK-6240 SUVR quantification, especially when HC with consistently high meningeal uptake or pathological cases with limited specific, cortical [ $^{18}F$ ]MK-6240 uptake are included for group comparison.

Even though PVC increased the variance of cortical SUVR, mainly in the aMCI group with 20 to 40% increases in coefficient of variation, both PVC approaches resulted in higher regional effect sizes with RBV PVC achieving the highest effect size, with an increase of 41%. These findings also indicated that RBV PVC is the preferred PVC approach for [ $^{18}F$ ]MK-6240 SUVR quantification in the context of group separation, as it allows for a higher discriminative accuracy for differentiation between aMCI and HC and a stronger correlation of [ $^{18}F$ ]MK-6240 SUVR with clinical scores. This improved effect size needs to be outweighed towards an increase in variability that is



of the same range in the context of detection of disease progression or drug monitoring studies. The current approach should thus also be investigated in a longitudinal data set to evaluate the variability of meningeal [ $^{18}\text{F}$ ]MK-6240 uptake within subjects on the one hand, and to assess the optimal balance between quantitative accuracy, improved effect size and increased variance due to the PVE correction method on the other hand.

In addition, we investigated the impact of PVC on the correlation of mesotemporal SUVR with a global cognitive MMSE score in the aMCI cohort, since tau uptake in the mesotemporal cortex is known to be related to this parameter.<sup>1</sup> Both PVC methods resulted in a stronger, highly significant correlation between mesotemporal SUVR and MMSE scores compared to no-PVC SUVR data, with RBV PVC demonstrating the most significant and strong correlation. This indicates that, despite the increased variance, the correlation strength improves and thus supports a PVC approach that may obtain most sensitive results for cognitive score versus tau binding correlations.

To obtain robust PVC results, optimal processing parameters such as the FWHM and an accurate segmentation and parcellation should be selected in the PVC algorithm.<sup>34</sup> It has been shown that incorrect specification of the FWHM results into systematic over- or underestimation of PVC SUVR data.<sup>35</sup> In this study, we used a FWHM of 6.5 mm to mimic the PET resolution of our scanner. Oyama et al. observed slightly different influences of FWHM mismatch on SUVR estimates in HC and AD groups.<sup>34</sup> Therefore, we also explored smaller FWHM down to 5 mm to assess group differences between HC groups. In our cohorts of HC, these analyses could not completely eliminate spill-in effects as differences were still observed in SUVR RBV data between two cohort of HC.

We examined alternative methods of parcellating regions by using a pseudo T1 approach<sup>36,37</sup> to determine the skull segment which contains the meningeal structure. Combination of the FreeSurfer parcellation with this pseudo T1 approach resulted in similar results, eliminating any potential bias introduced by the parcellation in our results.

Additionally, as meningeal uptake visually appeared to be heterogeneous within controls, an extended RBV PVC method was explored which also performed a parcellation of the skull to account for varying tracer uptake in the extracerebral compartment (Supplementary Materials and Methods). Results from this extended RBV PVC method were very similar to the RBV method (see Supplementary Table 2–3 and Supplementary Figure 4) and therefore, one can assume the extracerebral tracer uptake to be homogeneous for [ $^{18}\text{F}$ ]MK-6240 PVC quantification. As to the

exact origin of the off-target uptake and its impact on the current study, recently Gogola et al.<sup>15</sup> reported some off-target [ $^{18}\text{F}$ ]MK-6240 uptake in calcified/ossified extracerebral tissue. A possible contribution of spill-in effects of the skull could therefore be present, but this is however covered in our method as we selected a full skull compartment to model off-target extracerebral [ $^{18}\text{F}$ ]MK-6240 uptake that also encompassed this potential origin.

Limitations of the present study include the rather small sample size of our patient population. Another limitation is the need of a high-resolution brain MR image for PVC in the PET image. However, we assume that a clinical brain MR image is often present for patients with neurodegenerative diseases. Furthermore, our approach depends on the accurate segmentation of this MR image, which could be more problematic in later stages of the disease and should be carefully investigated in these populations.

In conclusion, this study demonstrated that subject-dependent meningeal uptake can have significant impact on cortical differences in [ $^{18}\text{F}$ ]MK-6240 SUVR between HC and aMCI and on the strength of clinical-biomarker correlations. To minimize PVE, we introduced a PVC algorithm that includes a correction for extracerebral spill-in effects which homogenizes control groups and produces a higher effect size to compare aMCI patients with HC, independent of off-target meningeal [ $^{18}\text{F}$ ]MK-6240 uptake especially in the control group.

## Funding

The author(s) disclosed receipt of the following financial support for the research, authorship, and/or publication of this article: This study was supported by an FWO grant (FWO/G093218N) and KU Leuven internal C2 funding (C24-17-063). NM is PhD mandate holder of the Fund for Scientific Research, Flanders, Belgium (FWO). RL is a senior clinical investigator of FWO Flanders.

## Acknowledgments

We thank all the participants for their willingness to participate in this study. The authors are grateful to the PET-MR technologists, in particular Kwinten Porters and Jef Van Look for their contribution in data acquisition. We also thank the PET radiopharmacy team and nuclear medicine medical physics team for their skilled contributions.


## Declaration of conflicting interests


The author(s) declared the following potential conflicts of interest with respect to the research, authorship, and/or publication of this article: KVL and MK have performed contract research through KU Leuven for Merck, Janssen Pharmaceuticals, UCB, Cerveau, Syndesi, Eikonizo, GE Healthcare and Curasen. All other authors declare that they have no conflict of interest.

## Authors' contributions

Conceptualization and designing work: NM, LM, KVL, MK.  
Data analysis and interpretation: NM, LM, KVL, MK.  
Critically revision of final version of manuscript: NM, LM,  
GV, MV, RL, KVL, MK.

## ORCID iDs

Nathalie Mertens  <https://orcid.org/0000-0002-2409-7586>

Laura Michiels  <https://orcid.org/0000-0002-1208-5334>

## Supplemental material

Supplemental material for this article is available online.

## References

1. Vanhaute H, Ceccarini J, Michiels L, et al. In vivo synaptic density loss is related to tau deposition in amnesic mild cognitive impairment. *Neurology* 2020; 95: e545–e553.
2. Wang YT and Edison P. Tau imaging in neurodegenerative diseases using positron emission tomography. *Curr Neurol Neurosci Rep* 2019; 19: 45.
3. Cho H, Choi JY, Hwang MS, et al. Tau PET in Alzheimer disease and mild cognitive impairment. *Neurology* 2016; 87: 375–383.
4. Leuzy A, Chiotis K, Lemoine L, et al. Tau PET imaging in neurodegenerative tauopathies – still a challenge. *Mol Psychiatry* 2019; 24: 1112–1134.
5. Tago T, Toyohara J, Harada R, et al. Characterization of the binding of tau imaging ligands to melanin-containing cells: putative off-target-binding site. *Ann Nucl Med* 2019; 33: 375–382.
6. Smith R, Schöll M, Leuzy A, et al. Head-to-head comparison of tau positron emission tomography tracers [18F]flortaucipir and [18F]RO948. *Eur J Nucl Med Mol Imaging* 2020; 47: 342–354.
7. Villemagne VL, Lopresti BJ, Dore V, et al. What is T+? A Gordian knot of tracers, thresholds & topographies. *J Nucl Med* 2021; 62: 614–619.
8. Lohith TG, Bennacef I, Vandenberghe R, et al. Brain imaging of Alzheimer dementia patients and elderly controls with 18F-MK-6240, a PET tracer targeting neurofibrillary tangles. *J Nucl Med* 2019; 60: 107–114.
9. Betthausen TJ, Cody KA, Zammit MD, et al. In vivo characterization and quantification of neurofibrillary tau PET radioligand [18F]MK-6240 in humans from Alzheimer's disease dementia to young controls. *J Nucl Med* 2019; 60: 93–99.
10. Pascoal TA, Shin M, Kang MS, et al. In vivo quantification of neurofibrillary tangles with [18F]MK-6240. *Alzheimers Res Ther* 2018; 10: 74.
11. Salinas C, Lohith TG, Purohit A, et al. Test–retest characteristic of [18F]MK-6240 quantitative outcomes in cognitively normal adults and subjects with Alzheimer's disease. *J Cereb Blood Flow Metab* 2020; 40: 2179–2187.
12. Guehl NJ, Wooten DW, Yokell DL, et al. Evaluation of pharmacokinetic modeling strategies for in-vivo quantification of tau with the radiotracer [18F]MK6240 in human subjects. *Eur J Nucl Med Mol Imaging* 2019; 46: 2099–2111.
13. Koole M, Lohith TG, Valentine JL, et al. Preclinical safety evaluation and human dosimetry of [18F]MK-6240, a novel PET tracer for imaging neurofibrillary tangles. *Mol Imaging Biol* 2020; 22: 173–180.
14. Kreisl WC, Lao PJ, Johnson A, et al. Patterns of tau pathology identified with 18F-MK-6240 PET imaging. *Alzheimer's Dement* 2021; : 1–11.
15. Gogola A, Minhas DS, Villemagne VL, et al. Direct comparison of the tau PET tracers [18F]flortaucipir and [18F]MK-6240 in human subjects. *J Nucl Med* 2022; 63: 108–116. Epub ahead of print DOI: 10.2967/jnumed.120.254961.
16. Walji AM, Hostetler ED, Selnick H, et al. Discovery of 6-(fluoro-18F)-3-(1H-pyrrolo[2,3-c]pyridin-1-yl)isoquinolin-5-amine ([18F]-MK-6240): a positron emission tomography (PET) imaging agent for quantification of neurofibrillary tangles (NFTs). *J Med Chem* 2016; 59: 4778–4789.
17. Hostetler ED, Walji AM, Zeng Z, et al. Preclinical characterization of 18F-MK-6240, a promising PET tracer for in vivo quantification of human neurofibrillary tangles. *J Nucl Med* 2016; 57: 1599–1606.
18. Aguero C, Dhaynaut M, Normandin MD, et al. Autoradiography validation of novel tau PET tracer [F-18]-MK-6240 on human postmortem brain tissue. *Acta Neuropathol Commun* 2019; 7: 37.
19. Collier TL, Yokell DL, Livni E, et al. cGMP production of the radiopharmaceutical [18F]MK-6240 for PET imaging of human neurofibrillary tangles. *J Labelled Comp Radiopharm* 2017; 60: 263–269.
20. Schramm G, Koole M, Willekens SMA, et al. Regional accuracy of ZTE-based attenuation correction in static [18F]FDG and dynamic [18F]PE2I brain PET/MR. *Front Phys* 2019; 7: 211.
21. Wu X. Optimal quantization by matrix searching. *J Algorithms* 1991; 12: 663–673.
22. Gronlund A, Larsen KG, Mathiasen A, et al. Fast exact k-Means, k-Medians and bregman divergence clustering in 1D. *arXiv* 2017; : 1801.07204.
23. Crary JF, Trojanowski JQ, Schneider JA, et al. Primary age-related tauopathy (PART): a common pathology associated with human aging. *Acta Neuropathol* 2014; 128: 755–766.
24. Michiels L, Mertens N, Thijs L, et al. Changes in synaptic density in the subacute phase after ischemic stroke: a 11C-UCB-J PET/MR study. *J Cereb Blood Flow Metab* 2021. Online ahead of print.
25. Müller-Gärtner HW, Links JM, Prince JL, et al. Measurement of radiotracer concentration in brain gray matter using positron emission tomography: MRI-based correction for partial volume effects. *J Cereb Blood Flow Metab* 1992; 12: 571–583.
26. Friston K, Ashburner J, Kiebel S, et al. *Statistical Parametric Mapping*. 2007.
27. Dahnke R, Gaser C. CAT-A Computational Anatomy Toolbox for the Analysis of Structural MRI Data. In: *22nd Annual Meeting of the Organization For Human Brain Mapping*, 2016.

28. Thomas BA, Erlandsson K, Modat M, et al. The importance of appropriate partial volume correction for PET quantification in Alzheimer's disease. *Eur J Nucl Med Mol Imaging* 2011; 38: 1104–1119.
29. Fischl B, van der Kouwe A, Destrieux C, et al. Automatically parcellating the human cerebral cortex. *Cereb Cortex* 2004; 14: 11–22.
30. Desikan RS, Ségonne F, Fischl B, et al. An automated labeling system for subdividing the human cerebral cortex on MRI scans into gyral based regions of interest. *Neuroimage* 2006; 31: 968–980.
31. Fischl B, Salat DH, Busa E, et al. Whole brain segmentation: Automated labeling of neuroanatomical structures in the human brain. *Neuron* 2002; 33: 341–355.
32. Wolters EE, Golla SSV, Timmers T, et al. A novel partial volume correction method for accurate quantification of [18F] flortaucipir in the hippocampus. *EJNMMI Res* 2018; 8: 79.
33. Maass A, Landau S, Baker SL, Alzheimer's Disease Neuroimaging Initiative, et al. Comparison of multiple tau-PET measures as biomarkers in aging and Alzheimer's disease. *Neuroimage* 2017; 157: 448–463.
34. Oyama S, Hosoi A, Ibaraki M, et al. Error propagation analysis of seven partial volume correction algorithms for [18F]THK-5351 brain PET imaging. *EJNMMI Phys* 2020; 7: 57.
35. Thomas BA, Cuplov V, Bousse A, et al. PETPVC: a toolbox for performing partial volume correction techniques in positron emission tomography. *Phys Med Biol* 2016; 61: 7975–7993.
36. Burgos N, Cardoso MJ, Thielemans K, et al. Attenuation correction synthesis for hybrid PET-MR scanners: Application to brain studies. *IEEE Trans Med Imaging* 2014; 33: 2332–2341.
37. Prados F, Cardoso MJ, Burgos N, et al. NiftyWeb: web based platform for image processing on the cloud. In: *Proceedings of the 24th Annual Meeting of ISMRM, Singapore: ISMRM*, 2016, p.2201.